JOURNAL OF SPACECRAFT AND ROCKETS
Vol. 32, No. 2, March–April 1995

Thermally Induced Vibrations of a Self-Shadowed Split-Blanket Solar Array

Earl A. Thornton,* Gregory P. Chini,† and David W. Gulick‡
University of Virginia, Charlottesville, Virginia 22903-2442

An analytical approach is developed for investigating thermally induced vibrations of a split-blanket solar array due to self-shadowing of the central truss. Two analyses are developed: 1) cross-member shadowing of the truss longerons due to a torsional vibration of the solar array, and 2) parallel-member shadowing when the solar vector is aligned with the plane of the truss longerons. The analytical approaches identify key parameters for understanding the thermal-structural response. For parallel-member shadowing a stability analysis establishes the condition for thermal flutter. Computations are made for a solar array representative of the Space Station Freedom (SSF) design. The results show that cross-member shadowing is unlikely to cause thermally induced vibrations. Parallel-member shadowing can cause thermally induced vibrations; however, the vibrations are stable. Under normal operations the SSF solar array should not experience thermally induced vibrations.

Nomenclature

A	= total longeron cross-sectional area ($A = 4d^2$), m^2
a	= central truss–solar-blanket separation distance, m (see Fig. 4)
a	= location of shadower projection upper edge, m [see Eq. (3e)]
b	= solar-blanket width, m (see Fig. 4)
b	= location of shadower projection lower edge, m [see Eq. (3)]
c	= longeron specific heat, J/kg-K
D	= shadower–shadowed member separation distance, m
d	= shadower cross-sectional width, m
EI	= equivalent beam flexural stiffness, N-m^2
F_x	= solar-blanket longitudinal tensile force, N/m
F_y	= solar-blanket transverse tensile force, N/m
GJ	= equivalent beam torsional stiffness, N-m^2
I_s	= spreader-bar mass moment of inertia, kg-m^2
I_x	= equivalent beam mass polar moment of inertia per unit length, kg-m
L	= solar-array length, m
M_s	= spreader-bar mass, kg
M_T	= thermal moment, N-m
M_x	= equivalent beam torque [see Eq. (10b)], N-m
M_y	= equivalent beam bending moment about y axis [see Eq. (11b)], N-m
m_x	= beam mass per unit length, kg/m
P	= central-truss axial compressive force, N
q	= torsional base excitation frequency, Hz
$\dot{q}_n$	= normal solar heat flux, W/m^2
$\dot{q}_s$	= solar heat flux, W/m^2
R_s	= radius of sun, m
$r(x)$	= mass moment-of-inertia distribution [see Eq. (22)], kg-m
S	= distance to sun, m
SHAD	= solar heat flux attenuation factor [see Eq. (4)]
T	= temperature, K
T_0	= initial temperature, K
T_q	= forced torsional oscillation period, s
V	= equivalent beam shear force, N
w	= displacement in z direction, m
x, y, z	= solar-array coordinates, m
α	= longeron absorptivity
α_T	= longeron coefficient of thermal expansion, K^{-1}
Γ	= truss eigenfunction, rad
γ	= truss cant angle, degrees
ΔT	= temperature difference between front and rear longerons, K
ε	= longeron emissivity
ζ	= damping ratio
η	= nondimensional stability parameter
θ	= truss angle of rotation about x axis, rad
θ_0	= amplitude of base torsional excitation, rad
θ_s	= solar flux incidence angle, rad
Λ	= solar-blanket eigenfunction, rad
ρ	= density, kg/m^3
σ	= Stefan-Boltzmann constant, W/m^2-K^4
σ_{sb}	= solar-blanket mass per unit area, kg/m^2
τ	= thermal response time, s
ϕ	= truss eigenfunction, m
ψ	= solar-blanket eigenfunction, m
Ω	= solar-array base excitation frequency, rad/s
ω	= solar-array natural frequency, rad/s

Subscripts

b	= equivalent beam
QS	= quasistatic
s	= spreader bar
sb	= solar blanket

Received Feb. 9, 1994; presented as Paper 94-1379 at the AIAA/ASME/ASCE/AHS/ASC 33rd Structures, Structural Dynamics, and Materials Conference, Hilton Head, SC, April 18–20, 1994; revision received June 7, 1994; accepted for publication June 9, 1994.

*Professor and Director, Light Thermal Structures Center. Associate Fellow AIAA.

†Undergraduate Research Assistant; currently Graduate Student, Cornell University, Ithaca, NY.

‡Undergraduate Research Assistant.

Introduction

THERMALLY induced vibrations of space structures are not a new phenomenon. Such oscillations became known in the 1960s during the flight of the OGO-IV spacecraft.[1] On that flight a 60-ft experiment boom sustained a solar-induced large-amplitude oscillation that severely compromised spacecraft performance. A detailed study of the problem showed that a coupled thermal-structural analysis predicted torsional-flexural oscillations consistent with the observed satellite behavior. Since then thermally induced vibrations of spacecraft appendages have been a recurrent problem. Reference 2 provides a historical description of the dynamic response of rapidly heated space structures, describes

thermal-structural analyses of spacecraft booms, and presents computations demonstrating unstable thermally induced vibrations.

In recent years several spacecraft have experienced thermally induced vibration problems; the most notable is the Hubble Space Telescope (HST). Shortly after the HST was deployed from the Space Shuttle Discovery in April 1990, a pointing "jitter" was observed. The jitter was subsequently traced to thermally induced motions of the solar arrays. Reference 3 describes investigations of the problem and presents an analysis of the thermally induced dynamic response. The analysis identifies design parameters that control the thermally induced vibration behavior. On the Space Shuttle Endeavor's mission in December 1993, new solar arrays designed to eliminate the persistent pointing jitter problem were installed.

Thermally induced oscillations typically occur on very low-frequency booms or solar arrays because of sudden heating changes at night-day transitions in the orbit. Sudden heating of an appendage may cause temperature changes that generate time-dependent bending moments that deform the structure. The appendage motion typically can be resolved into two components: 1) a relatively large-amplitude, slowly developing quasistatic motion, and 2) a superimposed transient vibratory motion consisting of contributions from one or more vibration modes. Since the spacecraft experiences no external forces or moments due to temperature changes, linear and angular momenta are conserved. Therefore, in response to an appendage deformation, the entire spacecraft responds dynamically with motions about the system mass center. These motions may degrade system performance either by undesirable displacements or by unexpected accelerations.

As in earlier designs, the most recent configuration of SSF uses multiple deployable split-blanket solar arrays. The solar arrays are cantilevered in pairs from the Space Station's main truss. Thermally induced motions of the solar arrays could degrade SSF's performance in several ways. One possibility is thermally induced structural accelerations that could adversely affect planned microgravity experiments.

The purpose of this paper is to describe a study of thermally induced vibrations of a split-blanket solar array for a typical night-day orbital transition. Analytical models are used to investigate thermally induced motions. The paper begins by discussing possibilities for thermally induced vibrations including self-shadowing effects. The approach for analyzing self-shadowing is described next. Following are free-vibration analyses for flexural and torsional modes of a solar array and membrane bending modes of the solar blankets. Then thermally induced motions due to cross-member and parallel-member shadowing are analyzed. Numerical results are presented for a split-blanket solar array representative of SSF designs.

Possibilities for Thermally Induced Vibration

An enlarged view of a SSF solar array is shown in Fig. 1. The major components of the deployed array are an extendable central truss, two pretensioned solar blankets consisting of membranes with solar cells attached to one side, and an end spreader bar that pulls the solar blankets from their storage boxes as the central truss is deployed from its storage canister. The central truss in its deployed configuration consists of four longerons, transverse battens, and crossed, pretensioned diagonal wires. Careful examination of Fig. 1 shows the central truss is oriented in a rotated, or canted, position. This rotation is evident in that all four longerons are visible from a view normal to the deployed solar blankets.

The bending and torsional behavior of the central truss determines the possibilities for thermally induced vibrations. Three such vibration scenarios are hypothesized. One possibility is that the longerons may develop temperature gradients over their cross sections. These gradients would induce thermal bending moments and transverse bending of the solar array. This behavior occurred on the original HST solar arrays.[3] For the SSF solar arrays, however, the longerons are made of a high thermal-conductivity aluminum alloy, and cross-section temperature gradients are negligible. Therefore, this scenario is unlikely to occur and will not be discussed further. Two other possibilities involve truss temperature gradients developing from slender-member shadowing, and these are investigated in detail. In the first shadowing scenario, the SSF main truss is assumed to

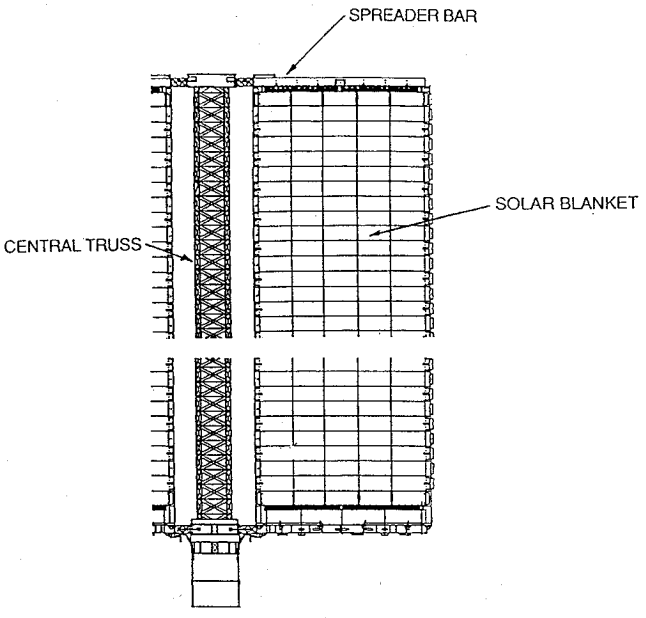

Fig. 1 Enlarged view of a Space Station solar array.

experience sustained bending vibrations that cause a torsional vibration of the solar array. Because of the torsional vibration, the front longerons (the longerons nearest the sun) shade the rear longerons on account of cross-member shadowing. The cross-member shadowing causes a temperature gradient across the truss cross section. The temperature gradient, in turn, produces a thermal bending moment, which induces flexural vibrations. In the second shadowing scenario, the front longerons are assumed to shade the rear longerons on account of parallel-member shadowing. Parallel-member shadowing occurs if the solar heat flux vector makes an incident angle to the solar panels equal to the cant angle. In the event of parallel-member shadowing, a truss cross-sectional temperature gradient develops. The resulting thermal bending and flexural vibrations of the solar arrays would be similar to the vibrations experienced on the HST.

Self-Shadowing

The heat flux on a structural member in Earth orbit depends on the orbit altitude and the member's orientation with respect to the sun and Earth. The heat flux $\dot{q}$ varies with time and is the sum of the solar heat flux $\dot{q}_s$, the Earth-emitted heat flux $\dot{q}_e$, and the Earth albedo heat flux $\dot{q}_a$. Member-to-member shadowing attenuates the solar heat flux on the shadowed member. Shadowing of Earth and albedo heating can be neglected because of the proximity and consequent large apparent size of the Earth. The attenuation of solar heating is represented by an attenuation factor, SHAD,[4] defined as the proportion of solar radiation that reaches a member. Thus when shadowing is considered, the total member heat flux is

$$\dot{q} = \text{SHAD} \cdot \dot{q}_s + \dot{q}_e + \dot{q}_a \tag{1}$$

If no shadowing occurs, SHAD = 1, but for complete shadowing, SHAD = 0. Its actual value is determined by calculating the percentage area of the solar disk that is covered by the projection of the shadower. SHAD depends on the distance D between the shadowed member and shadower, a shadower dimension d, the radius R_s of the sun, and the distance S to the sun.

For two longerons of the central truss, the shadowing geometry is shown in Fig. 2. Considering the projection of the shadower against the solar disk, the value s represents the width of the shadower projection and is given by

$$s = Sd/D \tag{2}$$

The coordinates a and b locate the shadower projection on the solar disk. The projection of the shadower may lie exactly along the centerline of the solar disk or above or below it. If the shadower

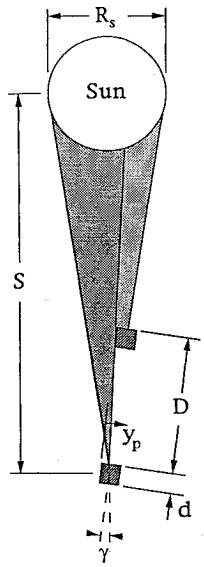

Fig. 2 Shadowing geometry for two longerons.

projection lies exactly on the centerline, then the lower edge of the projection is located by

$$b = R_s + s/2 \tag{3a}$$

For all other cases,

$$b = \frac{\alpha - \beta}{\alpha} R_s \tag{3b}$$

where

$$\alpha = \sin^{-1}(R_s/S) \tag{3c}$$

and

$$\beta = \gamma + \tan^{-1}(-y_p/D) \tag{3d}$$

in which γ is the cant angle. Once b is known, a is calculated from

$$a = b - s \tag{3e}$$

but if $b \geq 2R_s$ then we set $b = 2R_s$, and if $b < s$ then $a = 0$. Once a, b, and s are calculated, the shadowing attenuation factor, SHAD, is given by

$$\text{SHAD} = 1 - \frac{1}{\pi}\left\{\frac{1}{R_s^2}\left[(b - R_s)\sqrt{2bR_s - b^2} - (a - R_s)\sqrt{2aR_s - a^2}\right] + \left[\sin^{-1}\left(\frac{b - R_s}{R_s}\right) - \sin^{-1}\left(\frac{a - R_s}{R_s}\right)\right]\right\} \tag{4}$$

Figure 3 shows the variation of SHAD with y_p/d for various D/d ratios for a cant angle $\gamma = 0$. The figure shows that for the D/d ratio of the SSF central truss, shadowing of a rear longeron will occur. For example, near the center of the longeron at y_p/d equal to 0.5, the attenuation factor is zero. The attenuation factor integrated over the width d for a typical rear longeron indicates an average value of about 12%. In other words, there is about an 88% reduction of the heat flux on the rear longeron due to self-shadowing.

Structural Analysis

The mathematical model and coordinate system employed in subsequent analyses are shown in Fig. 4. The structural equations of motion assume: 1) the centroidal axis of the central truss and the midplane of the solar blankets lie in the the xy plane, 2) the central truss may be represented by a cantilevered Bernoulli-Euler beam with equivalent flexural stiffness EI, 3) the central truss in subjected to a constant compressive force P due to pre-tension of the solar blankets, 4) the central truss in torsion may be represented by a beam with torsional stiffness GJ, 5) the solar blankets may be represented by membranes with constant, uniform tensile in-plane forces F_x and F_y per unit length, 6) the transverse membrane force F_y is small compared to the longitudinal membrane force F_x, 7) solar-blanket thermal deformations are neglected, and 8) the spreader bar is rigid and supports the membrane tensile forces F_x over a length b for each solar blanket. Equilibrium of forces on the spreader bar in the x direction requires $P = 2bF_x$. Based on these assumptions, analytical models are developed for the dynamic analyses.

Equations of Motion

The structural analysis uses equations of motion for the central truss, the solar blankets, and the spreader bar. The equations are solved subject to boundary conditions at the cantilevered support and continuity conditions with the spreader bar. The approach is similar to the formulation presented in Ref. 6 except that in the present study thermal effects are included, and a different solar-blanket membrane formulation is used.

The flexural equation of motion for the central truss modeled as a beam is

$$\text{EI}\frac{\partial^4 w_b}{\partial x^4} + P\frac{\partial^2 w_b}{\partial x^2} + \frac{\partial^2 M_T}{\partial x^2} + m_x\frac{\partial^2 w_b}{\partial t^2} = 0 \tag{5}$$

where the thermal moment M_T is defined by

$$M_T(x,t) = \int_A E\alpha_T\,\Delta T z\,dA \tag{6}$$

The torsional equation of motion for the central truss is

$$\text{GJ}\frac{\partial^2\theta}{\partial x^2} = I_x\frac{\partial^2\theta}{\partial t^2} \tag{7}$$

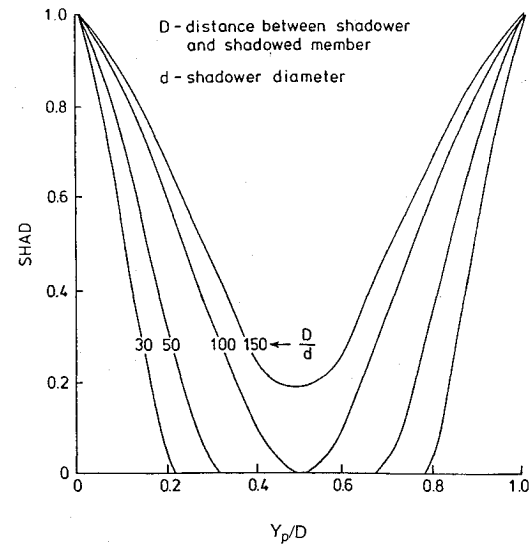

Fig. 3 Variation of SHAD across a longeron for various *D/d* ratios.

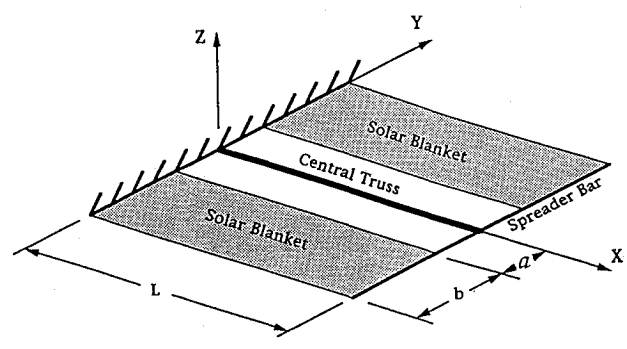

Fig. 4 Mathematical model of a solar array.

The equation of motion of a solar blanket is

$$F_x \frac{\partial^2 w_{sb}}{\partial x^2} + F_y \frac{\partial^2 w_{sb}}{\partial y^2} = \sigma_{sb} \frac{\partial^2 w_{sb}}{\partial t^2} \tag{8}$$

and the translational equation of motion of the spreader bar is

$$V(L,t) + 2\int_a^{b+a} F_x \frac{\partial w_{sb}}{\partial x}(L,y,t)\,dy + M_s \frac{\partial^2 w_s}{\partial t^2} = 0 \tag{9a}$$

where V is defined by

$$V = -EI\frac{\partial^3 w_b}{\partial x^3} - P\frac{\partial w_b}{\partial x} - \frac{\partial M_T}{\partial x} \tag{9b}$$

The rotational equation of motion of the spreader bar is

$$M_x(L,t) + \int_{-(b+a)}^{-a} F_x \frac{\partial w_{sb}}{\partial x}(L,y,t)y\,dy + \int_a^{b+a} F_x \frac{\partial w_{sb}}{\partial x}(L,y,t)y\,dy + I_s \frac{\partial^2 \theta}{\partial t^2}(L,t) = 0 \tag{10a}$$

where the beam torque is defined by

$$M_x = GJ\frac{\partial \theta}{\partial x} \tag{10b}$$

Boundary and Continuity Conditions

The beam's flexural boundary and continuity conditions are

$$\begin{gathered} w_b(0,t) = 0 \\ \frac{\partial w_b}{\partial x}(0,t) = 0 \\ w_b(L,t) = w_s(t) \\ M_y(L,t) = 0 \end{gathered} \tag{11a}$$

where

$$M_y = -EI\frac{\partial^2 w_b}{\partial x^2} - M_T \tag{11b}$$

The beam's torsional boundary and continuity conditions are

$$\begin{gathered} \theta(0,t) = 0 \\ \theta(L,t) = \theta_s(t) \end{gathered} \tag{11c}$$

The boundary and continuity conditions for the solar blankets at the base and at the spreader bar are

$$w_{sb}(0,t) = 0 \tag{12a}$$

$$w_{sb}(L,y,t) = y\theta(L,t) \tag{12b}$$

On the free edges of the solar blankets the boundary conditions require the membrane forces F_y to be zero. Moreover, rigorous determination of the membrane force distributions requires solution of a plane stress problem[7] for $F_x(x,y)$ and $F_y(x,y)$. In the present analysis, the membrane forces are assumed constant. The force F_x is specified by the pretensioning, and F_y is assumed small but nonzero. In Refs. 3 and 6, F_y is neglected and only membrane flexural vibration modes with deformations independent of y are permitted. Here, F_y is retained so that membrane modes with deformations as a function of y may be included. With F_y constant and nonzero, approximate boundary conditions on the free edges are assumed. For the typical solar blanket for $y > 0$, the boundary condition is

$$\frac{\partial w_{sb}(x,a,t)}{\partial y} = \frac{\partial w_{sb}(x,a+b,t)}{\partial y} \tag{13}$$

with a similar boundary condition on the other solar blanket (i.e., $y < 0$). These boundary conditions permit free edge deflections while insuring that the small edge forces are self-equilibrating. Equilibrium of forces in the y direction will be satisfied for each solar blanket, and equilibrium of moments about the x axis will be satisfied for the pair of solar blankets.

Truss Buckling

Since the truss is subjected to the compressive force P, buckling may occur. The critical Euler buckling force is the same as that for a simply supported beam, since the line of action of the force P passes through the end supports. Thus

$$P_{cr} = n^2\pi^2\frac{EI}{L^2}, \qquad n = 1,2,3,\ldots \tag{14}$$

Normally the compressive force P is a small percentage of P_{cr}.

Vibration Modes

Study of the free-vibration behavior shows there are three classes of vibration modes: 1) flexural vibrations of the central truss and solar blankets, where motions are symmetric about the xz plane and solar-blanket deformations are independent of y, 2) torsional vibrations of the central truss and solar blankets about the x axis, and 3) membrane bending modes of the solar blankets with the central truss and the spreader bar motionless.

Flexural Modes

Vibration frequencies and mode shapes are determined by solving Eqs. (5) and (8) subject to the boundary conditions given in Eqs. (11a) and (12) and neglecting thermal effects. Assuming

$$w_b = \phi(x)\sin\omega t$$

$$w_{sb} = \psi(x)\sin\omega t$$

the analysis yields

$$\phi(x) = \frac{D_1}{D_2}\sin\delta x - \cos\delta x - \frac{D_1}{D_2}\frac{\delta}{\varepsilon}\sinh\varepsilon x + \cosh\varepsilon x \tag{15a}$$

$$\psi(x) = \phi(L)\frac{\sin(\sqrt{\sigma_{sb}/F_x}\,\omega x)}{\sin(\sqrt{\sigma_{sb}/F_x}\,\omega L)} \tag{15b}$$

where

$$\begin{aligned} D_1 &= \delta^2\cos\delta L + \varepsilon^2\cosh\varepsilon L \\ D_2 &= \delta^2\sin\delta L + \delta\varepsilon\sinh\varepsilon L \end{aligned} \tag{15c}$$

and

$$\begin{aligned} \delta &= \left\{\frac{P}{2EI}\left[\left(1 + \frac{4m_x\omega^2 EI}{P^2}\right) + 1\right]\right\}^{\frac{1}{2}} \\ \varepsilon &= \left\{\frac{P}{2EI}\left[\left(1 + \frac{4m_x\omega^2 EI}{P^2}\right) - 1\right]\right\}^{\frac{1}{2}} \end{aligned} \tag{15d}$$

For free vibrations the frequency equation is derived by substituting Eqs. (15a) and (15b) into the spreader-bar translational equation of motion, Eq. (9a). Then

$$EI\phi'''(L) + P\phi'(L) - P\psi'(L) + M_s\omega^2\phi(L) = 0 \tag{16}$$

where a prime denotes differentiation with respect to x. For a given force P, Eq. (16) is solved numerically to obtain the flexural frequencies.

Torsional Modes

The torsional vibration frequencies and mode shapes are determined by solving Eqs. (7) and (8) subject to the boundary conditions given in Eqs. (11c) and (12). Assuming

$$\theta = \Gamma(x)\sin\omega t$$

$$w_{sb} = y\Lambda(x)\sin\omega t$$

the analysis yields

$$\Gamma(x) = \sin\sqrt{I_x/GJ}\,x \tag{17a}$$

$$\Lambda(x) = \frac{\sin(\sqrt{I_x/GJ}\,\omega L)\sin(\sqrt{\sigma_{sb}/F_x}\,\omega x)}{\sin(\sqrt{\sigma_{sb}/F_x}\,\omega L)} \tag{17b}$$

The frequency equation is derived by substituting Eqs. (17) into the spreader-bar rotational equation of motion, Eq. (10a). Then after performing the indicated integrations

$$GJ\Gamma'(L) + \tfrac{2}{3}F_x[(b+a)^3 - a^3]\Lambda'(L) - I_s\Gamma(L)\omega^2 = 0 \qquad (18)$$

where as before a prime denotes differentiation with respect to x. For a given membrane force, Eq. (18) is solved numerically to obtain the torsional frequencies.

Solar-Blanket Modes

Solar-blanket vibration modes occur with the central truss and spreader bar motionless. The vibration modes are obtained by solving the membrane equation of motion, Eq. (8), subject to appropriate boundary conditions. The membranes must have zero deflection at the centilever base and at the spreader bar; on the free edges, the boundary condition given in Eqs. (13) is imposed. Assuming $F_y \ll F_x$ and taking

$$w_{sb} = \psi(y)\sin\frac{m\pi x}{L}\sin\omega t, \qquad m = 1, 2, \ldots$$

the analysis yields for the solar blanket with $y > 0$,

$$\psi(y) = c_1 + c_2 y, \qquad n = 0 \qquad (19a)$$

$$\psi(y) = \cos\frac{n\pi}{b}(y - a), \qquad n = 1, 2, 3, \ldots \qquad (19b)$$

and the natural frequencies are given by

$$\omega_{mn} = \pi\sqrt{\frac{m^2F_x}{L^2\sigma_{sb}} + \frac{n^2F_y}{b^2\sigma_{sb}}} \qquad (20)$$

There is a similar set of eigenfunctions for the solar blanket with $y < 0$. The vibration shapes of the solar blankets must be considered as a pair with natural frequencies given by Eq. (20). Vibrations of the solar blankets are considered together to insure that rotational equilibrium of the spreader bar, Eq. (10), is satisfied. In computations, F_y is assumed much smaller than F_x, since the lateral edges of the solar blankets are actually free.

Cross-Member Shadowing

Cross-member shadowing may occur if the solar array experiences a torsional oscillation. To study the possibility of cross-member shadowing, a periodic rotational base motion of the solar array is assumed. Such a base motion could be caused by a flexural motion of SSF's main truss. The analysis of cross-member shadowing proceeds by deriving the solar array's response to the prescribed base motion. Then, an approach for determining the shadowing events is presented. Finally, an analysis of the thermal response to cross-member shadowing is developed.

Torsional Response

The base of the solar array (Fig. 4) is assumed to undergo periodic excitation

$$\theta(0, t) = \theta_0 \sin\Omega t$$
$$w_{sb}(0, y, t) = y\theta_0 \sin\Omega t \qquad (21)$$

The torsional response is determined by solving Eqs. (7–8) using the vibration modes given in Eq. (17). The solution is the sum of two parts: a quasistatic motion of the massless system, and a relative motion caused by the inertial forces. The first part is the rigid-body motion of the system due to the base motion. The second part is a modal expansion in terms of the eigenfunctions. The coefficients in the modal expansion are evaluated using the orthogonality condition,

$$\int_0^L r(x)\Gamma_m(x)\Gamma_n(x)\,dx + \int_0^L r_{sb}\Lambda_m(x)\Lambda_n(x)\,dx = 0 \qquad (22a)$$

a) Undeformed central truss—no shadowing

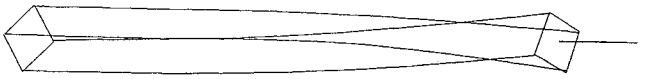

b) Torsionally deformed central truss—cross member shadowing

Fig. 5 Distortion of the central truss during torsional oscillations.

for $m \neq n$. The weighting functions $r(x)$ and r_{sb} are the distributions of the mass moments of the inertia for the central truss, spreader bar, and solar blankets,

$$r(x) = I_x + I_s\delta(x - L)$$
$$r_{sb} = I_{sb} = \tfrac{2}{3}[(b+a)^3 - a^3]\sigma_{sb} \qquad (22b)$$

where $\delta(x - L) = 0$ for $0 < x < L$, and $\delta(x - L) = 1$ for $x = L$. With equivalent viscous damping, the steady-state periodic solution is given by

$$\theta(x, t) = \theta_0 \sin\Omega t + \theta_0 \sum_{n=1}^{\infty} a_n\Gamma_n(x)\frac{\Omega^2\cos(\Omega t - \phi_n)}{\sqrt{\left(\omega_n^2 - \Omega^2\right)^2 + 4\zeta^2\omega_n^2\Omega^2}} \qquad (23a)$$

The coefficient a_n and the phase angle ϕ_n are defined by

$$a_n = \frac{I_x\int_0^L \Gamma_n\,dx + I_s\Gamma_n(L) + I_{sb}\int_0^L \Lambda_n\,dx}{I_x\int_0^L \Gamma_n^2\,dx + I_s\Gamma_n^2(L) + I_{sb}\int_0^L \Lambda_n^2\,dx} \qquad (23b)$$

and

$$\phi_n = \tan^{-1}\left(\frac{\Omega^2 - \omega_n^2}{2\zeta\Omega\omega_n}\right) \qquad (23c)$$

The second term in Eq. (23a) represents the torsional distortion of the central truss and depends on the damping ratio ζ and the ratio of the excitation frequency Ω to the natural frequencies ω_n. A similar equation for the solar-blanket displacement $w_{sb}(x, t)$ could be derived, but it is not required for the cross-member shadowing analysis.

Shadowing Analysis

Cross-member shadowing is a transient phenomenon that occurs as the four-longeron truss oscillates near a resonance frequency because of the base excitation. Figure 5 shows a typical truss distortion at one time in the oscillation. The shadowing analysis is performed over an oscillation period by following the positions of the front and rear longerons. At the beginning and the end of an oscillation period, there is no cross-member shadowing, because the central truss is canted, but during an oscillation period cross sections of the truss may rotate through angles equal to or greater than the cant angle. As a truss cross section rotates through the cant angle, a front longeron shades a rear longeron as they come into alignment with the solar vector. A section near $x = L$ comes into alignment first, and other sections for $x < L$ come into alignment as the oscillation proceeds. Hence a shadowed region of the rear longeron moves inward from $x = L$ along the longeron to some minimum position as the vibration approaches its peak amplitude. Then the shadowed segment moves back towards $x = L$ as the vibration amplitude decreases. In the present analysis, shadowing is assumed to occur when the truss rotation angle θ at a section falls in the range of the cant angle $\gamma \pm \varepsilon$, where ε is a small angle. With this criterion, at a particular instant of time the minimum and maximum x values of the shaded segment of a rear longeron can be determined. Over this segment, an average SHAD factor is used, based on the D/d ratio of the truss and Fig. 3.

Thermal Analysis

Because of cross-member shadowing, there is a reduction of the incident heat flux on a segment of a rear longeron. The heat flux reduction is transient, as it occurs only over a short interval of the oscillation period, but it occurs periodically as the truss rotates cyclically through the forced torsional oscillation. To assess the temperature drop experienced by a shadowed segment, a crude but conservative thermal model is used. Each shadowed segment is assumed to be isothermal; that is, axial conduction in a longeron is neglected. Conservation of energy for a shaded segment then requires

$$\frac{dT}{dt} = \frac{\alpha}{\rho c d}\,\mathrm{SHAD}\,\dot{q}_s - \frac{4\sigma\varepsilon}{\rho c d}T^4 \tag{24}$$

where $T(t)$ is the temperature of the isothermal shaded segment. Equation (24) is solved subject to an initial condition $T(0) = T_0$, where T_0 is the initial temperature of the unshadowed segment. Numerical computations are required to determine the magnitude of the temperature decrease due to cross-member shadowing. Predicted temperature changes are described in the Numerical Results section.

Parallel-Member Shadowing

Parallel-member shadowing occurs if the solar array is oriented so that the solar vector makes an angle to the xz plane (Fig. 4) equal to the cant angle. If this orientation exists as the spacecraft makes the night-day transition in the orbit, then a temperature gradient will develop between the front, heated longerons and the rear, shaded longerons. Under these circumstances thermally induced vibrations will occur. A formulation for thermally induced vibrations due to parallel-member shadowing is developed assuming coupling between the incident heat flux and deforming structure.

Thermal Analysis

The beam model for the deformed central truss with the incident solar heat flux $\dot{q}_s$ is shown in Fig. 6. To provide generality, the solar heat flux vector is inclined by the angle θ_s. In writing the conservation-of-energy equations for the longerons, the heat flux absorbed is the component normal to the surface. Because of bending, a normal to the beam surface has rotated through a small angle equal to the beam slope. Thus, the incident normal solar heat flux to the surface varies with x along the beam and can be expressed by

$$\dot{q}_n = \dot{q}_s \cos\left(\theta_s - \frac{\partial w_b}{\partial x}\right) \tag{25}$$

Assuming each longeron is isothermal, conservation of energy may be written for a unit length of each member. Combining the equations for a front and rear longeron pair gives an equivalent single equation for the temperature difference $\Delta T = T_f - T_r$, where T_f denotes the temperature of the front longeron, and T_r denotes the temperature of the rear longeron. The combined energy equation is

$$\frac{d(\Delta T)}{dt} = \frac{\alpha(1 - \mathrm{SHAD})\dot{q}_n}{\rho c d} - \frac{4\sigma\varepsilon}{\rho c d}\left(T_f^4 - T_r^4\right) \tag{26}$$

which is solved subject to an initial condition $\Delta T(0) = 0$. The transient response begins as the spacecraft makes the night-to-day transition. For the first few minutes, as the members are heated rapidly by the solar flux, radiation heat losses are relatively small, and as an approximation radiation can be neglected. Substituting Eq. (25) in the approximate Eq. (26) gives

$$\frac{d(\Delta T)}{dt} = \frac{\alpha(1 - \mathrm{SHAD})\dot{q}_s}{\rho c d}\cos\left(\theta_s - \frac{\partial w_b}{\partial x}\right) \tag{27}$$

This result is a coupled differential equation for the longeron temperature difference that depends on the beam slope.

For the truss cross section, the thermal moment may be evaluated from Eq. (6). Taking into account the cant angle γ, the thermal moment about the y axis is

$$M_T = E\alpha_T DA\cos\gamma\,\Delta T/4 \tag{28}$$

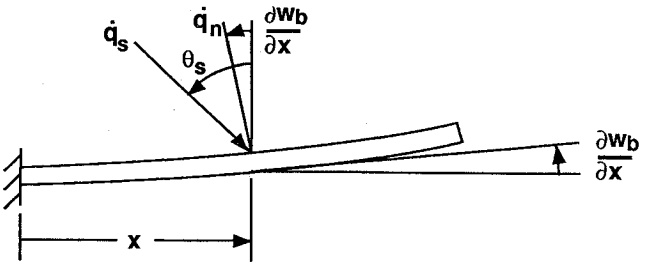

Fig. 6 Heat flux for coupled thermal-structural analysis.

where $A = 4d^2$. Combining the last two equations yields

$$M_T(x,t) = \frac{E\alpha_T DA\cos\gamma}{4}\,\frac{\alpha(1 - \mathrm{SHAD})\dot{q}_s}{\rho c d} \times \int_0^t \cos\left(\theta_s - \frac{\partial w_b}{\partial x}\right) dt \tag{29}$$

where Eq. (27) has been expressed in integral form taking into account the initial condition.

Structural Analysis

The thermal structural boundary–initial value problem consists in solving the solar-array flexural equations of motion (5) and (8) with the thermal moment given in Eq. (29). Since the thermal moment depends on the beam slope, a modal representation of the response cannot be obtained. Instead an approximate solution based on the method of weighted residuals (MWR) is developed.

The solutions for the central-truss and solar-blanket deflections are taken in the form

$$\begin{aligned} w_b(x,t) &= N_b(x)U(t) \\ w_{sb}(x,t) &= N_{sb}(x)U(t) \end{aligned} \tag{30}$$

where the approximating functions N_b and N_{sb} are assumed to satisfy the conditions

$$\begin{aligned} N_b(0) &= 0, \qquad & N_{sb}(0) &= 0 \\ N_b'(0) &= 0, \qquad & N_{sb}(L) &= N_b(L) \end{aligned}$$

where a prime denotes differentiation with respect to x. These functions are nondimensional to allow the time function $U(t)$ to represent the deflection of the array end as a function of time.

Following standard MWR procedures[3] yields an ordinary differential equation for $U(t)$,

$$\ddot{U} + \omega_0^2 U = F(t)/M \tag{31a}$$

where $\omega_0 = \sqrt{K/M}$ is an approximation to the first-mode natural frequency and

$$K = \mathrm{EI}\int_0^L (N_b'')^2\,dx - P\int_0^L (N_b')^2\,dx + P\int_0^L (N_{sb}')^2\,dx \tag{31b}$$

$$M = m_x\int_0^L N_b^2\,dx + 2b\sigma_{sb}\int_0^L N_{sb}^2\,dx + M_s N_b^2(L) \tag{31c}$$

$$F(t) = -\int_0^L N_b'' M_T\,dx \tag{31d}$$

where K, M, and F are the stiffness, mass, and force, respectively, for the equivalent single-degree-of-freedom system. Equation (31a) remains difficult to solve because $F(t)$ in Eq. (31d) contains the unknown function $U(t)$ in the thermal moment M_T. The approach followed in Ref. 3 used the Laplace transform. With this approach a stability criterion for the dynamic response can also be derived.

Table 1 SSF solar-array data

Central truss	Value	Unit
L	32.92	m
P	667.2	N
m_x	4.211	kg/m
I_x	0.7853	kg-m
EI	4.821×10^6	N-m^2
GJ	1.366×10^5	N-m^2
d	0.01270	m
D	0.7620	m
ρ	6527	kg/m^3
c	895	J/kg-K
α	0.7	—
ε	0.8	—
γ	10.0	deg
α_T	23.6×10^{-6}	°C^{-1}
Solar blankets		
a	1.190	m
b	4.394	m
F_x	75.92	N/m
F_y	0.09110	N/m
σ_{sb}	1.170	kg/m^2
Spreader bar		
M_s	76.35	kg
I_s	794.0	kg-m^2
Solar		
$\dot{q}_s$	1390	W/m^2
R_s	1.435×10^9	m
S	1.498×10^{11}	m

The stability of the response is determined by obtaining the Laplace transform of Eq. (31a) and applying the Routh–Hurwitz stability criterion. With equivalent viscous damping and substitution for the thermal moment using Eq. (29), the equation of motion becomes

$$\ddot{U} + 2\zeta\omega_0\dot{U} + \omega_0^2 U = F(t)/M \tag{32a}$$

where

$$F(t) = -C\int_0^L \int_0^t N_b'' \cos\left(\theta_s - \frac{\partial w_b}{\partial x}\right) dt\, dx \tag{32b}$$

and

$$C = \frac{E\alpha_T DA\cos\gamma}{4}\frac{\alpha(1-\text{SHAD})\dot{q}_s}{\rho c d} \tag{32c}$$

Equation (32b) can be linearized by assuming that the beam's slope is small, so that

$$\cos\left(\theta_s - \frac{\partial w_b}{\partial x}\right) = \cos\theta_s - \frac{\partial w_b}{\partial x}\sin\theta_s$$

With this approximation and substituting Eq. (30), the equation of motion can then be written as

$$\ddot{U} + 2\zeta\omega_0\dot{U} + \omega_0^2 U + \left(\frac{C\sin\theta_s \int_0^L N_b' N_b''\, dx}{M}\right)\int_0^t U(t)\, dt = -\frac{C\cos\theta_s \int_0^L N_b''\, dx}{M} t \tag{33}$$

After performing the Laplace transformation, the characteristic equation that determines the stability of the system is

$$q(s) = s^3 + 2\zeta\omega_0 s^2 + \omega_0^2 s + \frac{C\sin\theta_s \int_0^L N_b' N_b''\, dx}{M} \tag{34}$$

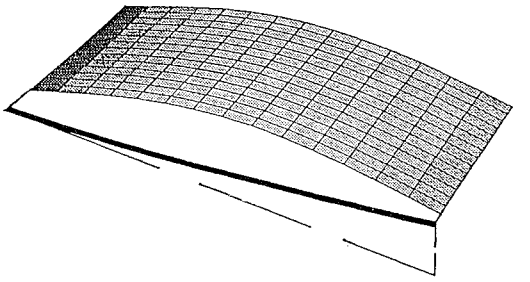

a) First mode, f_1 = 0.115 Hz

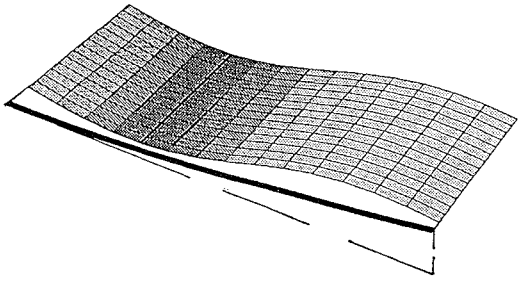

b) Second mode, f_2 = 0.222 Hz

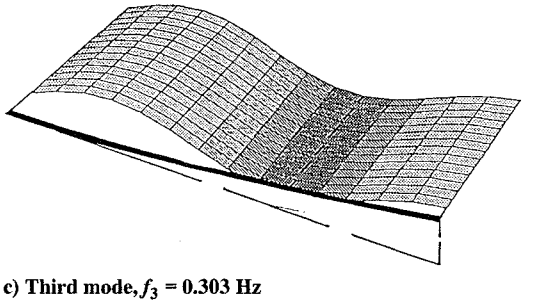

c) Third mode, f_3 = 0.303 Hz

Fig. 7 Solar-array flexural modes (only central truss and one array are shown).

For a stable solution, the Routh–Hurwitz stability criterion requires

$$2\zeta\omega_0^3 > \frac{C\sin\theta_s \int_0^L N_b' N_b''\, dx}{M} \tag{35}$$

This last result may be written in nondimensional form by introducing the nondimensional parameters

$$\frac{1}{\tau} = \frac{4\sigma\varepsilon T_R^3}{\rho c d} \tag{36a}$$

$$\eta = \frac{\alpha_T T_R}{D}\left(\frac{\text{EI}}{K}\int_0^L N_b' N_b''\, dx\right)\cos\gamma\sin\theta_s \tag{36b}$$

$$\kappa = 1/\omega_0\tau \tag{36c}$$

where

$$T_R = \left[\frac{\alpha(1-\text{SHAD})\dot{q}_s}{4\sigma\varepsilon}\right]^{\frac{1}{4}} \tag{36d}$$

and $I = AD^2/4$. Note that I is a principal moment of inertia and is independent of the cant angle. Then the stability criterion can be written as

$$\eta < \frac{2\zeta}{\kappa} \tag{37}$$

Equation (37) indicates that the stability of the response becomes critical when

$$\eta_{cr} = \frac{2\zeta}{\kappa}$$

This critical value represents the boundary between stable and unstable responses.

Because ζ and κ are always positive quantities, η_{cr} is always positive. However, when the solar vector incidence angle θ_s is zero or negative, Eq. (36b) shows that the parameter $\eta \leq 0$. Thus for these orientations of the solar vector, thermally induced vibrations are always stable. However, for $\theta_s > 0$ the coupled thermal structural vibrations may be unstable, i.e., thermal flutter may occur. These results are consistent with previous results for cantilever beams[2] and the HST solar arrays.[3]

Numerical Results

The numerical results use data (Table 1) representative of a SSF solar array.

Vibration Modes

Flexural and torsional vibration frequencies and mode shapes were computed for the solar array using the data from Table 1. The first three modes for flexure and torsion are shown in Figs. 7 and 8, respectively. In addition, several solar-blanket modes were computed, and typical results are shown in Fig. 9. The flexural and torsional modes are characterized by simultaneous distortion of the central truss and the solar blankets. In contrast, there is a large family of solar-blanket modes that occur without distortion of the central truss. While these modes are in the frequency range of the flexural and torsional modes, the solar-blanket modes will not be excited by thermal gradients. Thermal gradients will excite only the modes associated with thermal distortions of the central truss. Note that all modes are of rather low frequency; the nine modes shown are in the range of 0.1 to 0.3 Hz. Some frequencies, such as the first modes in torsion and flexure, are quite close together (0.115 and 0.114 Hz, respectively).

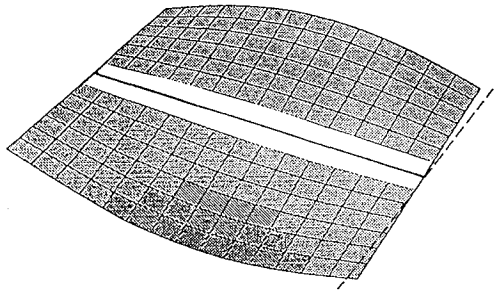

a) First mode, f_1 = 0.114 Hz

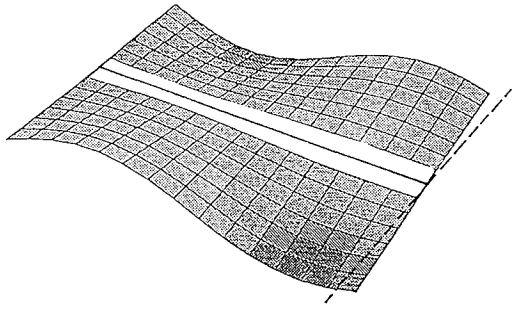

b) Second mode, f_2 = 0.224 Hz

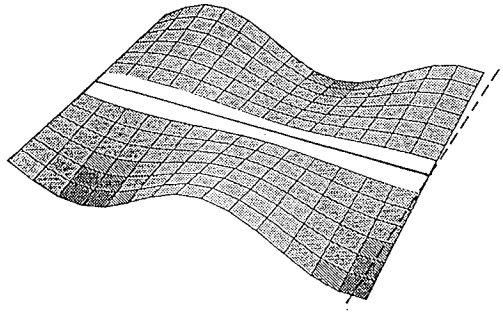

c) Third mode, f_3 = 0.321 Hz

Fig. 8 Solar-array torsional modes.

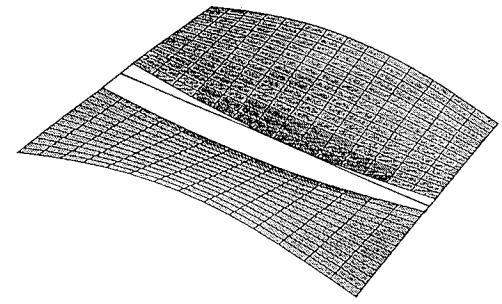

a) First mode, f_1 = 0.122 Hz

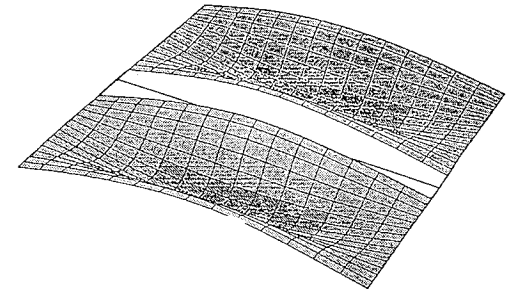

b) Second mode, f_2 = 0.138 Hz

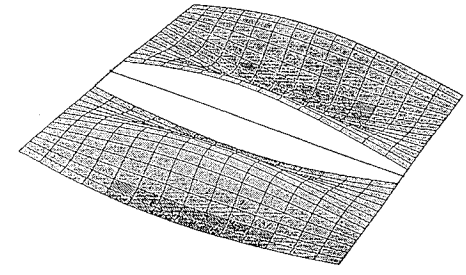

c) Third mode, f_3 = 0.152 Hz

Fig. 9 Solar-blanket modes.

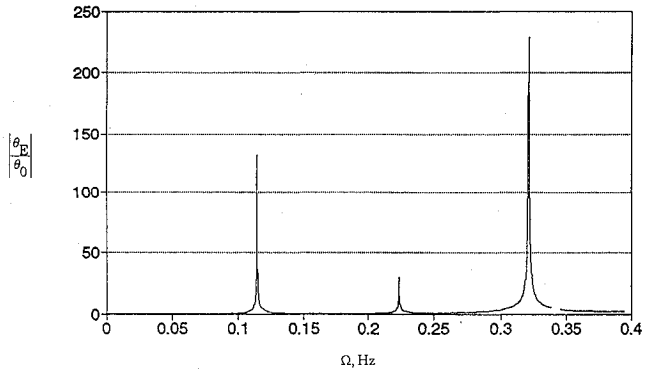

Fig. 10 Solar-array frequency response (maximum elastic amplification) to torsional excitation, $\xi = 0.1\%$.

Cross-Member Shadowing

To investigate the possibility of cross-member shadowing, the response of the solar array to a harmonic base excitation was computed

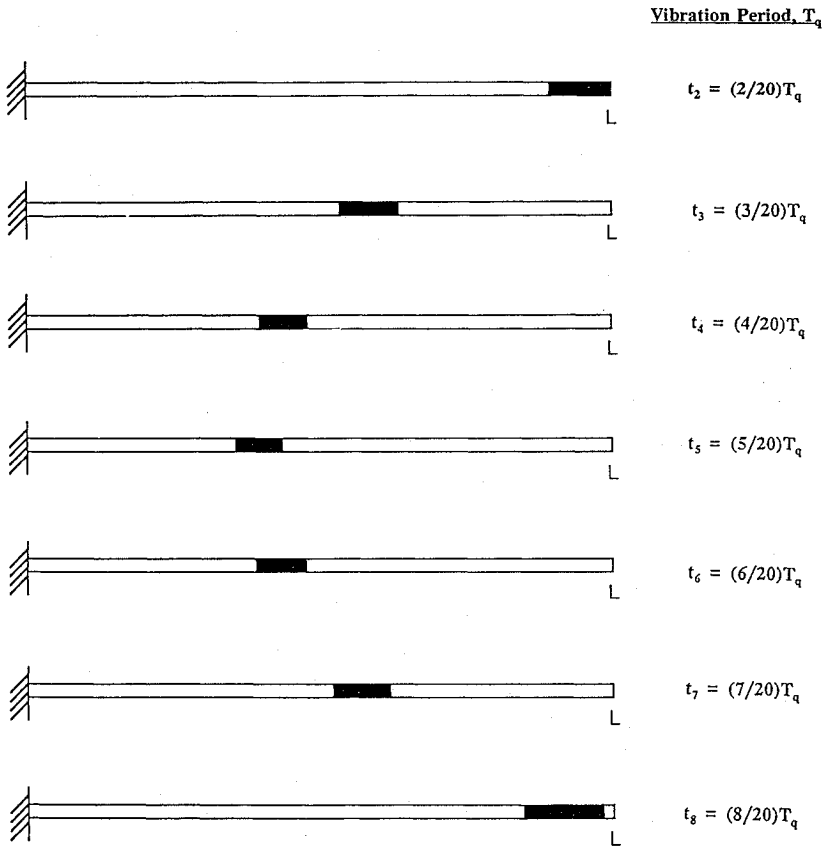

Fig. 11 Cross-member shadowing during torsional oscillation, $\theta_0 = 5$ deg, $q_1 = 0.109$ Hz, $T_q = 9.2$ s.

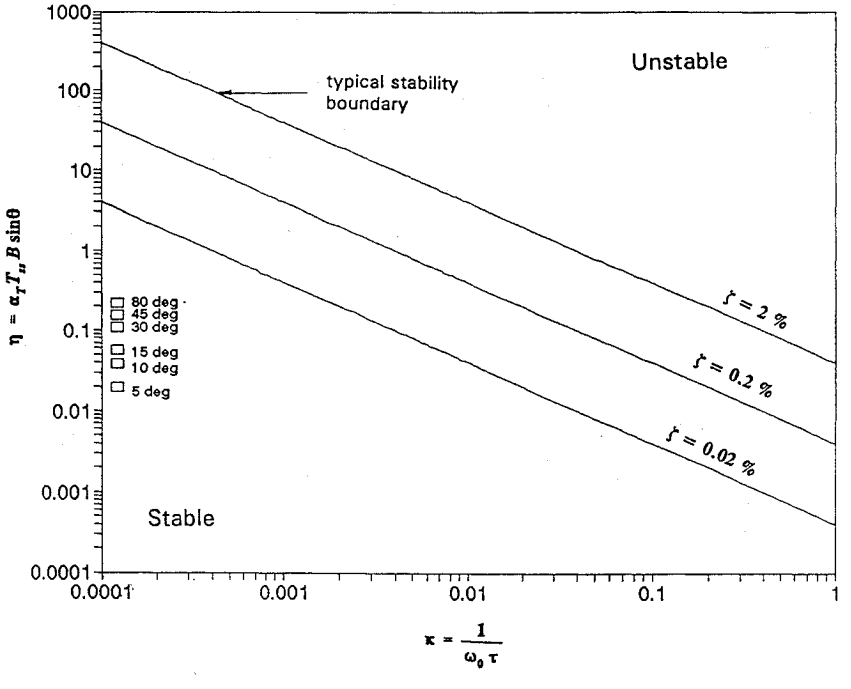

Fig. 12 Stability boundaries for SSF split-blanket solar array.

using Eq. (23). The magnitude of the elastic portion of the response θ_E normalized to the magnitude of the base motion θ_0 is plotted versus the excitation frequency Ω for a damping ratio $\zeta = 0.1\%$ in Fig. 10. As expected, large elastic deformations occur near the resonant frequencies.

To assess the cross-shadowing occurrences, the solar array was excited harmonically for $q_1 = 0.95 f_1$ and $\theta_0 = 5$ deg, where f_1 is the frequency of the first torsional mode. For shadow determination, $\gamma = 10 \pm 0.5$ deg was used. The shadow lengths and movements are shown in Fig. 11. The first point to observe is that the shadowed segments represent only a small portion of a longeron length, typically about $10\%L$. The second point is that because of the shadow movement, a longeron segment experiences a reduction in solar flux for only a small portion of the oscillation period. For example, in Fig. 11 the segment of the longeron near $x = L$ is shadowed at most for about $\frac{4}{20}$ of the period T_q, or about 1.8 s. For the balance of the

oscillation period, the segment receives the full solar flux. Computation of the temperature drop during the 1.8 s of shadowing using Eq. (24) showed that the temperature decrease is quite small. Therefore, there is little possibility that a thermal moment will be created by cross-member shadowing. Consequently, thermally induced oscillations due to cross-member shadowing are highly unlikely to occur.

Parallel-Member Shadowing

The coupled thermal-structural analysis depends on selection of the approximating functions $N_b(x)$ and $N_{sb}(x)$ used in Eq. (30). Based on the experience with the HST,[3] the eigenfunctions for the first mode, Eqs. (15), were selected, as they satisfy all boundary conditions and yield a good approximation for the first-mode frequency. With these functions selected, the various integrals that define parameters such as K in Eq. (31b), M in Eq. (31c), and η in Eq. (36b) may be evaluated.

Using the stability criterion given in Eq. (37), the stability boundaries for the coupled thermal-structural response of a solar array are shown in Fig. 12. On the vertical axis of the figure is the nondimensional parameter η, which is a measure of the thermally induced response. Equation (36b) shows η is proportional to the coefficient of thermal expansion α_T, a shaded longeron radiation temperature T_R, the cosine of the cant angle γ, and the sine of the angle θ_s that measures the inclination of the solar vector from the vertical (see Fig. 6). Recall that for $\theta_s \leq 0$, the response is unconditionally stable. The nondimensional parameter κ, which is a measure of the structural response time in relation to the thermal response time, is on the horizontal axis. The three curves shown for the damping ratios $\zeta = 0.02$, 0.002, and 0.0002 are the stability boundaries. For a given damping ratio, designs below a stability boundary are stable, and designs above are unstable. The figure shows that damping is a critical factor; increased damping corresponds to a larger region of stable vibrations. Shown in the figure with square symbols are η and κ values for the SSF solar array for $\gamma = 0$ and $\theta_s = 5$ through 80 deg. The solar-array designs can experience thermally induced vibrations due to parallel-member shadowing, but the vibrations will be stable and will decay with time.

In normal operations, the SSF split-blanket solar arrays will be operated so that the central truss is oriented with a 10-deg cant angle, and the solar vector will be nearly normal to the solar blankets. This study shows that under these conditions thermally induced vibrations are highly unlikely to occur.

Concluding Remarks

Analytical models have been used to investigate thermally induced vibrations of a split-blanket solar array for a typical night-day orbital transition. The solar array employs a four-longeron central truss. Three possibilities for thermally induced vibrations were considered based on thermal bending moments developing due to 1) longeron cross-sectional temperature gradients, 2) longeron cross-member shadowing due to torsional vibrations, and 3) longeron parallel-member shadowing. The first possibility can be avoided by using solid longerons of high thermal conductivity or by insulating the longerons and was not investigated further. The second and third possibilities were investigated in detail.

A shadowing analysis was presented, and an approach for computing the attenuation of solar heating was described for both cross- and parallel-member shadowing. For geometry representative of the solar-array central truss on SSF, up to 88% reduction in solar heating can occur due to shadowing.

An analysis of the solar-array vibration behavior was made using classical beam and membrane theory. The vibration modes fall into three classes: 1) combined flexural modes of the central truss and solar blankets, 2) combined torsional modes of the central truss and solar blankets, and 3) flexural modes of the solar blankets with the central truss stationary. Only the flexural and torsional modes of the first two classes have a role in thermally induced motions. Nine modes are predicted between 0.1 and 0.3 Hz, and the first-mode flexural and torsional frequencies are nearly identical.

An analysis of cross-member shadowing due to forced torsional oscillations of the solar array predicts shadow lengths and motions during a typical vibration period. For SSF solar-array geometry the cross-shadow lengths and durations are small and would not cause any appreciable temperature gradient to develop across the truss cross section. Therefore, thermally induced vibrations due to cross-member shadowing are very unlikely to occur.

Parallel-member shadowing can cause thermally induced vibrations. An analysis of parallel-member shadowing develops an approach for predicting the dynamic response, taking into account thermal-structural coupling. A stability criterion given in nondimensional parameters establishes the conditions for which thermal flutter of the solar array may occur. Computations for the SSF solar array showed that if parallel-member shadowing occurs, the vibrations are stable. For the planned SSF solar-array design, the central truss is canted so that parallel-member shadowing cannot occur under normal operations.

The analytical approach provides insight into possible thermally induced vibration behavior of a split-blanket solar array and identifies key design features as well as parameters that are important for understanding the thermally induced response. For shadowing effects, the size and the spacing of the slender members are important as might be expected. The truss member material and surface properties determine the thermal response time. Significant structural properties include the stiffness of the central truss and the thermal expansion coefficient. Key parameters in determining thermal flutter include the ratio of the thermal and structural response times, solar inclination angles, and system damping.

Acknowledgments

The research efforts of the authors were supported in part by the Light Thermal Structures Center through a grant from the University of Virginia Academic Enhancement Program. Additional support was provided by the Virginia Space Grant Consortium. We are very pleased to recognize the efforts of Yool A. Kim, who is currently a graduate student at MIT. While at UVA, she contributed significantly to the early phases of this study.

References

[1]Thornton, E. A., and Paul, D. B., "Thermal-Structural Analysis of Large Space Structures: An Assessment of Recent Advances," *Journal of Spacecraft and Rockets*, Vol. 22, No. 4, 1985, pp. 385–393.

[2]Thornton, E. A., and Foster, R. S., "Dynamic Response of Rapidly Heated Space Structures," *Computational Nonlinear Mechanics in Aerospace Engineering*, edited by S. N. Atluri, Vol. 146, Progress in Astronautics and Aeronautics, AIAA, Washington, DC, 1992, pp. 451–477.

[3]Thornton, E. A., and Kim, Y. A., "Thermally Induced Bending Vibrations of a Flexible Rolled-Up Solar Array," *Journal of Spacecraft and Rockets*, Vol. 30, No. 4, 1993, pp. 438–448.

[4]Mahaney, J., and Thornton, E. A., "Self-Shadowing Effects on the Thermal-Structural Response of Orbiting Trusses," *Journal of Spacecraft and Rockets*, Vol. 24, No. 4, 1987, pp. 342–348.

[5]O'Neill, R. F., and Zich, J. L., "Space Structure Heating: A Numerical Procedure for Analysis of Shadowed Space Heating of Sparse Structures," in *Spacecraft Radiative Transfer and Temperature Control*, edited by T. E. Horton, Progress in Astronautics and Aeronautics, AIAA, New York, Vol. 83, 1982, pp. 377–395.

[6]Carney, K. S., and Shaker, F. J., "Free Vibration Characteristics and Correlation of a Space Station Split-Blanket Solar Array," AIAA Paper 89-1252, NASA TM 101452, April 1989.

[7]Leonard, J. W., *Tension Structures—Behavior and Analysis*, McGraw–Hill, 1988, pp. 205–220.

E. V. Zoby
Associate Editor